Redox Biology 73 (2024) 103215

Contents lists available at ScienceDirect

Redox Biology

journal homepage: www.elsevier.com/locate/redox

FOXO1 regulates RUNX2 ubiquitination through SMURF2 in calcific aortic valve disease

Chen Jiang [a,1], Dingyi Yao [a,1], Zongtao Liu [a,1], Yidan Zheng [a,1], Ming Chen [a], Wai Yen Yim [a], Qiang Zheng [a], Tailong Zhang [a], Lin Fan [a], Zhengfeng Fan [a], Bingchuan Geng [a], Rui Tian [a], Tingwen Zhou [a], Weihua Qiao [a], Jiawei Shi [a], Fei Li [a,**], Li Xu [a,***], Yuming Huang [b,****], Nianguo Dong [a,*]

[a] Department of Cardiovascular Surgery, Union Hospital, Tongji Medical College, Huazhong University of Science and Technology, Wuhan, Hubei, 430022, China
[b] Department of Thoracic Surgery, The First Affiliated Hospital of Nanjing Medical University, Nanjing, Jiangsu, 210029, China

ARTICLE INFO

Keywords:
Calcific aortic valve disease
Forkhead box O1
Phosphorylation
SMAD-Specific E3 ubiquitin ligase 2
Ubiquitination

ABSTRACT

The prevalence of calcific aortic valve disease (CAVD) remains substantial while there is currently no medical therapy available. Forkhead box O1 (FOXO1) is known to be involved in the pathogenesis of cardiovascular diseases, including vascular calcification and atherosclerosis; however, its specific role in calcific aortic valve disease remains to be elucidated. In this study, we identified FOXO1 significantly down-regulated in the aortic valve interstitial cells (VICs) of calcified aortic valves by investigating clinical specimens and GEO database analysis. FOXO1 silencing or inhibition promoted VICs osteogenic differentiation in vitro and aortic valve calcification in Apoe$^{-/-}$ mice, respectively. We identified that FOXO1 facilitated the ubiquitination and degradation of RUNX2, which process was mainly mediated by SMAD-specific E3 ubiquitin ligase 2 (SMURF2). Our discoveries unveil a heretofore unacknowledged mechanism involving the FOXO1/SMURF2/RUNX2 axis in CAVD, thereby proposing the potential therapeutic utility of FOXO1 or SMURF2 as viable strategies to impede the progression of CAVD.

1. Introduction

Calcific aortic valve disease (CAVD) is the prevailing heart valve disease in Western societies [1]. The incidence of CAVD rises significantly with advancing age [2,3]. Given the escalating surgical demands among the elderly population, the imperative to develop efficacious pharmaceutical interventions to impede or reverse CAVD progression underscores the criticality of investigating the pathogenesis of CAVD.

Currently, CAVD is regarded as a progressive and irreversible ailment influenced by various factors. The pathogenesis encompasses endothelial injury, lipid accumulation, inflammation, and even cellular senescence [4]. The subsequent pathological phase involves the transformation of valvular interstitial cells (VICs) into myofibroblast-like and osteoblast-like cells [5]. Consequently, impeding the osteogenic differentiation of VICs emerges as a pivotal strategy to mitigate CAVD.

The osteogenic differentiation process of VICs involves a variety of regulatory mechanisms among which runt-related transcription factor 2 (RUNX2) is recognized as the primary transcription regulator [6]. The PI3K/AKT signaling pathway is considered crucial for osteoblast differentiation [7,8] and has been implicated in vascular calcification

* Corresponding authors. Department of Cardiovascular Surgery, Union Hospital of Tongji Medical College, Huazhong University of Science and Technology, Wuhan Jiefang Road, No.1277, Hubei, 430022, China.
** Corresponding author. Department of Cardiovascular Surgery, Union Hospital, Tongji Medical College, Huazhong University of Science and Technology, Wuhan Jiefang Road, No.1277, Hubei, 430022, China.
*** Corresponding authors. Department of Cardiovascular Surgery, Union Hospital, Tongji Medical College, Huazhong University of Science and Technology, Wuhan Jiefang Road, No.1277, Hubei, 430022, China.
**** Corresponding author. Department of Thoracic Surgery, The First Affiliated Hospital of Nanjing Medical University, Nanjing Guangzhou Road, No.300, Jiangsu, 210029, China.
E-mail addresses: lifei_union@sina.com (F. Li), whunionxl@163.com (L. Xu), doctor-huangym@foxmail.com (Y. Huang), 1986XH0694@hust.edu.cn (N. Dong).
[1] These authors contributed equally to this work.

https://doi.org/10.1016/j.redox.2024.103215
Received 19 April 2024; Received in revised form 16 May 2024; Accepted 24 May 2024
Available online 27 May 2024

through its regulation of RUNX2 [9–11]. Forkhead Box O1 (FOXO1), plays important role in PI3K/AKT signaling pathway [9,10], has been shown to have significant involvement in various disease fields [11]. FOXO1 not only interacts with the RUNX2 protein but also plays a role in atherosclerosis and vascular calcification [12–18]. However, the extent to which FOXO1 can regulate and interact with RUNX2 during the osteogenesis of VICs remains uncertain.

This study reveals that FOXO1 is down-regulated in calcific aortic valves and, in vitro, it facilitates the ubiquitination and degradation of RUNX2 via SMAD-specific E3 ubiquitin ligase 2 (SMURF2), thereby impeding the osteogenic differentiation of VICs. Therefore, targeting FOXO1 or SMURF2 could potentially serve as an innovative therapeutic approach for CAVD.

2. Methods

2.1. Human samples and ethics

Control non-calcified aortic valve was obtained from patients undergoing cardiac transplantation due to dilated cardiomyopathy, and the calcified aortic valve was obtained from patients undergoing aortic valve replacement due to CAVD. This study complied with the Helsinki Declaration and was approved by the System Review Committee of Tongji Medical College of Huazhong University of Science and Technology. Written informed consents were obtained before surgeries.

2.2. Western blot analysis

Proteins were extracted using radioimmunoprecipitation assay (RIPA) buffer (New Cell & Molecular Biotech, WB3100) containing protease and phosphatase inhibitor cocktail (New Cell & Molecular Biotech, P002). The bicinchoninic acid (BCA) protein assay kit (Beyotime Biotechnology, P0011) was used to determine the protein lysate concentrations. For western blotting, equal quantities of proteins from each group were electrophoresed by 4%–12 % sodium dodecyl sulfate polyacrylamide gel electrophoresis (ACE Biotechnology, ET15412Gel). Subsequently, the proteins were transferred onto polyvinylidene fluoride (PVDF) membranes (Millipore, 03010040001) and blocked with 5 % nonfat dry milk in Tris-buffered saline with 0.5 % Triton X-100 (TBS-T). The membranes were then probed with the indicated primary antibodies overnight at 4 °C, followed by incubation with the corresponding secondary antibodies for 1 h. Ultimately, the protein blots were developed using the enhanced chemiluminescence (New Cell & Molecular Biotech, P002), and the labeled bands were quantified by Image J 1.8 (National Institutes of Health).

2.3. Quantitative real-time polymerase chain reaction (qRT-PCR) assay

RNA of VICs was isolated using Total RNA Isolation Kit (Vazyme, RC112-01). cDNA was synthesized using the HiScript III RT SuperMix (Vazyme, R323-01) according to the manufacturer's instructions. RT-qPCR was conducted in optical 96-well plates using SYBR qPCR Master Mix (Vazyme, Q711-02) and a Step One Real-Time PCR System (Applied Biosystems, Foster City, CA, USA) according to the manufacturer's instructions. GAPDH was used as the internal control. Analysis of relative gene expression data was carried out using the ΔΔCt method. All primer sequences are listed in Table S2.

2.4. Bulk RNA sequencing analysis

All bulk RNA sequencing (RNA-seq) rawdata of three-tricuspid aortic valve were downloaded from European Nucleotide Archive and their information is available on Gene Expression Omnibus (GSE76718, GSE153555 and GSE148219). Rawdata underwent quality control (via Fastqc0.11.9), mapping (via Hisat2 v2.2.1) and qualification (via featureCounts v2.0.1) on Linux, to obtain the count matrix. The matrix was then filtered with compute counts per million (cpm) > 0 (edgeR) and then underwent normalization and the different expressed genes (DEGs) were acquired (via DESeq2) on R 4.2.1.

2.5. Single-cell RNA-seq analysis

Previously published single cell sequencing (scRNA-seq) data from Gene Expression Omnibus database (GSE180278) was included for reanalysis. Male mice with Ldlr (n = 24) or Apoe knocked out (n = 19) and fed a western diet for 8–10 weeks were categorized as hyperlipidemia model, and wild type C57BL/6J mice (n = 30) fed with chow diet were selected as control in comparison. Aortic valves from mice were collected for scRNA sequence after sacrifice.

Raw reads obtained from the 10 × Genomics single-cell RNA-seq platform were demultiplexed and mapped to the mice reference genome mm10 using the CellRanger software (version 3.0.2) with default parameters. Cells were removed under the condition of expressing fewer than 200 genes or greater than 20 % mitochondrial genes. R package Seurat (version 4.2.0) were used to perform dimensional reduction of scRNA-seq data. The "NormalizeData" and "ScaleData" function from Seurat was used for normalization, then followed by "FindVariableFeatures" to calculate highly variable genes. "FindIntegrationAnchors" in the Seurat package were applied to remove batch effect and integrate data. 2000 genes with the highest expression and dispersion from each sample were determined as the integration anchors and used for integration. Then, cells were projected in 2D space using Uniform Manifold Approximation and Projection (UMAP). To identify differentially expressed genes (DEGs) among each cluster, the "FindAllMarkers" function from Seurat was used and non-parametric Wilcoxon rank sum tests were set to evaluate the significance of each individual DEG. DEGs with adjusted P value less than 0.05 were thought to be significant and used in downstream analysis. Hierarchical clustering and heatmap generation were performed for single cells on the basis of normalized expression values of marker genes curated from the literature or identified significant DEGs. "DimPlot" and "VlnPlot" were used to visualize the expression of individual genes, cells were grouped by their cell type as determined by analysis with Seurat. Pathway enrichment was performed by 'fgsea' R package (version 1.27.1). Gene set was extracted from 'MH' geneset in 'msigbr' R package (version 7.5.1). Transcriptional factor list was download from TRRUST version 2 (https://www.grnpedia.org/trrust/).

Plot polish was performed by R package SCP (version 0.5.6), in which 'Integration_SCP', 'FeatureDimPlot', 'RunDEtest', 'CellDimPlot', 'AnnotateFeatures' functions were called for modification.

2.6. Hematoxylin and eosin (H&E) staining

Briefly, paraffin-embedded sections of aortic valves were dewaxed and dehydrated. After washing with distilled water, the sections were then stained with Harris' modified hematoxylin solution for 3 min. Then the sections were washed with running tap water for 5 min, followed by counterstaining in eosin alcoholic solution for 1 min. Finally, the sections were dehydrated in increasing concentrations of ethyl alcohol and cleared in xylene for 2 min.

2.7. Von Kossa staining

Generally, aortic valve leaflets were dewaxed, dehydrated and incubated with 5 % silver nitrate solution for 30 min. Then, the sections were exposed directly to bright sunshine for 1 h, washed, and treated with 5 % sodium sulfate for 2 min. After restaining with neutral red for another 3 min, the deposition of calcium salt in the aortic valve leaflets was observed using a light microscope. A threshold value of the reflection intensity was defined to isolate mineralized nodules from the background using Image J 1.8 (National Institutes of Health), and the total mineralized area was calculated.

2.8. Alizarin Red staining

For tissue: Aortic valve leaflets were fixed in 4 % PFA overnight, then dehydrated by 15 % and 30 % sucrose solution, washed in distilled water and stained with 2 % Alizarin Red stain (Sigma-Aldrich) for 30–60 min. After staining, the valves were washed in distilled water again.

For cell: After treatments, VICs were rinsed in 1 × PBS, then fixed in 4 % PFA for 15 min at room temperature and rinsed in distilled water. The fixed cells were stained with 0.2 % Alizarin Red stain (Servicebio, G1038-100 ML) for 30 min and then washed in distilled water. For quantification, the area of Alizarin Red positive field was calculated using Image J 1.8 (National Institutes of Health) and averaged for independent biological replicates. Images were visualized and captured using an Olympus microscope. The calcium concentration was measured colorimetrically by the o-cresolphthalein method in 0.1 mol/L hydrochloric acid extracts from cultured VICs. The calcium content was expressed as microgram calcium per well of a 12 well plate.

2.9. Immunohistochemistry staining

Generally, after antigen retrieval, paraffin sections of aortic valve tissues were incubated with the primary antibody overnight at 4 °C, followed by incubation with an HRP-conjugated secondary antibody. Images were taken with a fluorescence microscope (Carl Zeiss, Jena, Germany) and merged using Image J 1.8 (National Institutes of Health).

2.10. Immunofluorescence staining

After being dried at room temperature for 20 min, frozen sections of aortic valves were fixed in 4 % PFA for 30 min and then permeabilized with 0.1 % Triton X-100 in PBS for another 15 min. Next, the tissues were incubated with the primary antibody, followed by incubation with fluorescently conjugated secondary antibody and counterstaining with 4′,6-diamidino-2-phenylindole (DAPI).

2.11. Cell culture

Human aortic VICs were isolated from noncalcified aortic valves as described previously [19,20]. Briefly, after washing the aortic valves three times in PBS, they were digested in 1 mg/mL type I collagenase for 12 h at 37 °C in 5 % CO_2. Subsequently, the cell suspension was gently spun for 10 min at 1000 rpm, then the resuspended, separated primary VICs were cultured in high glucose Dulbecco's modified Eagle's medium (DMEM, Gibco, Invitrogen, Carlsbad, CA, USA) supplemented with 10 % fetal bovine serum (Gibco) in a humidified atmosphere with 5 % CO2 at 37 °C. VICs at subcultures 3 to 5 were used for further studies. Osteogenic differentiation of VICs was induced in osteogenic medium (OM) comprising DMEM supplemented with 2 % fetal bovine serum, 1 % penicillin–streptomycin, 10 mmol/L of β-glycerophosphate, 0.1 μmol/L of dexamethasone, and 50 μg/mL ascorbic acid. Unless otherwise specified, OM was treated for 3 days for cellular Western blot assay, 21 days for cellular Alizarin red staining, and 2 months for ex-vivo valves osteogenic differentiation model. The OM was replenished every 3 days. All experiments were performed on VICs from independent batches (n values represent different experiments).

2.12. Experimental animals and protocols

All animal procedures complied with the Guide for the Care and Use of Laboratory Animals published by the US National Institutes of Health (NIH Publication No. 85-23, revised 1996) and were approved by the Animal Care and Use Committee of Tongji Medical College. *Apoe*$^{-/-}$ mice, were purchased from Shulaibao Biotechnology Co., Ltd. (Wuhan, China).

Eight-week-old male *Apoe*$^{-/-}$ (n = 20) were randomly allocated to 2 groups (n = 10 each group): (1) mice fed with western diet and vehicle; (2) mice fed with western diet supplemented with AS1842856 (10 mg/kg) for 24 weeks. All the mice were housed in a pathogen-free, temperature-controlled environment under a 12-h light/dark cycle. After 24 weeks, hemodynamic parameters were determined by transthoracic echocardiography using an 18–38 MHZ phased-array probe (MS400) connected to a Vevo 2100 Imaging system under 2.5 % isoflurane anesthesia. After that, the mice were euthanized by intravenous injection of a lethal dose of pentobarbital sodium (100 mg/kg). Mice were then perfused via the left ventricle with 5 ml PBS prior to tissue collection. Mice hearts were carefully dissected and embedded.

2.13. Masson's trichrome staining

Generally, after fixing in acetone-methanol for 10 min, the mouse aortic valves were immersed in a Weigert iron hematoxylin solution for 5 min. The slides were rinsed again in running tap water for 5 min. Then, the sections were incubated in 0.02 % azophloxine and 0.04 % acid fuchsin solution for 20 min and rinsed with 1 % acetic acid solution. Next, they were placed in a 2.5 % phosphotungstic acid solution for 10 min and rinsed with 1 % acetic acid solution. Finally, the sections were dehydrated in ethanol and xylene, cleared in toluene solutions, and then mounted using a quick-hardening mounting medium. The fractional areas of collagen fibrosis components (blue) in the aortic valve region were obtained using Image J 1.8 (National Institutes of Health).

2.14. Coimmunoprecipitation (co-IP)

Briefly, upon reaching 60–70 % confluency, VICs cultured in 100 mm dishes were treated with MG132 for 8 h before the indicated treatments. Medium was then removed and cells were washed with PBS, then lysed with 1 ml of chilled IP lysis buffer (New Cell & Molecular Biotech, P70100). Cell lysate was then collected in a 1.5 mL Eppendorf tube and centrifuged for 15 min at 12,000 rpm at 4 °C, and the supernatant was transferred to a new tube. The protein concentration of the supernatant was measured by using a BCA protein assay kit (Beyotime Biotechnology, P0010) to quantify protein concentration. The samples were then adjusted with lysis buffer to prepare 1 mg protein per IP and 20 μg protein per input. The IP antibody or normal IgG were bind to the Protein A/G PLUS Agarose (Santa Cruz Biotechnology, sc-2003) following the manufacturer's instruction. Then, 1 mg of proteins was transferred into the beads that have been linked to IP antibody or normal human IgG. The samples were mixed and incubated for overnight at 4 °C with rotation at 20 rpm to perform IP. Following formation of the beads-antibody-antigen complex, samples were centrifuged for 5 min at 3500 rpm at 4 °C to remove the supernatant. The beads were then re-suspended in 700 μl lysis buffer and repeated centrifugation to remove supernatant. After final washing, the complex pellet was re-suspended in 100 μl 1 × electrophoresis buffer. The collected sample was then heated at 95 °C for 15 min and then subjected to SDS-PAGE analysis and immunoblotting.

2.15. Adenovirus-mediated overexpression

Recombinant adenovirus vectors of indicated gene were designed and purchased from WZ Biosciences Inc. (Shandong, China). VICs were seeded at the density of 1.0×10^5 cells/well in 6-well plates and incubated with adenovirus at 50 MOI (see Figure S3 for MOI value screening experiment). After 48 h of incubation with adenovirus, VICs were used for subsequent interventions, including OM as well as others.

2.16. Small interfering RNA-mediated silencing

siRNAs targeting FOXO1, SMURF2 and the negative control siRNA (si-NC) with no definite target were designed and synthesized by RiboBio. (Guangzhou, China). The siRNA sequences are listed in Supplementary Table S2. Briefly, VICs were seeded on 6-well plates 24 h prior

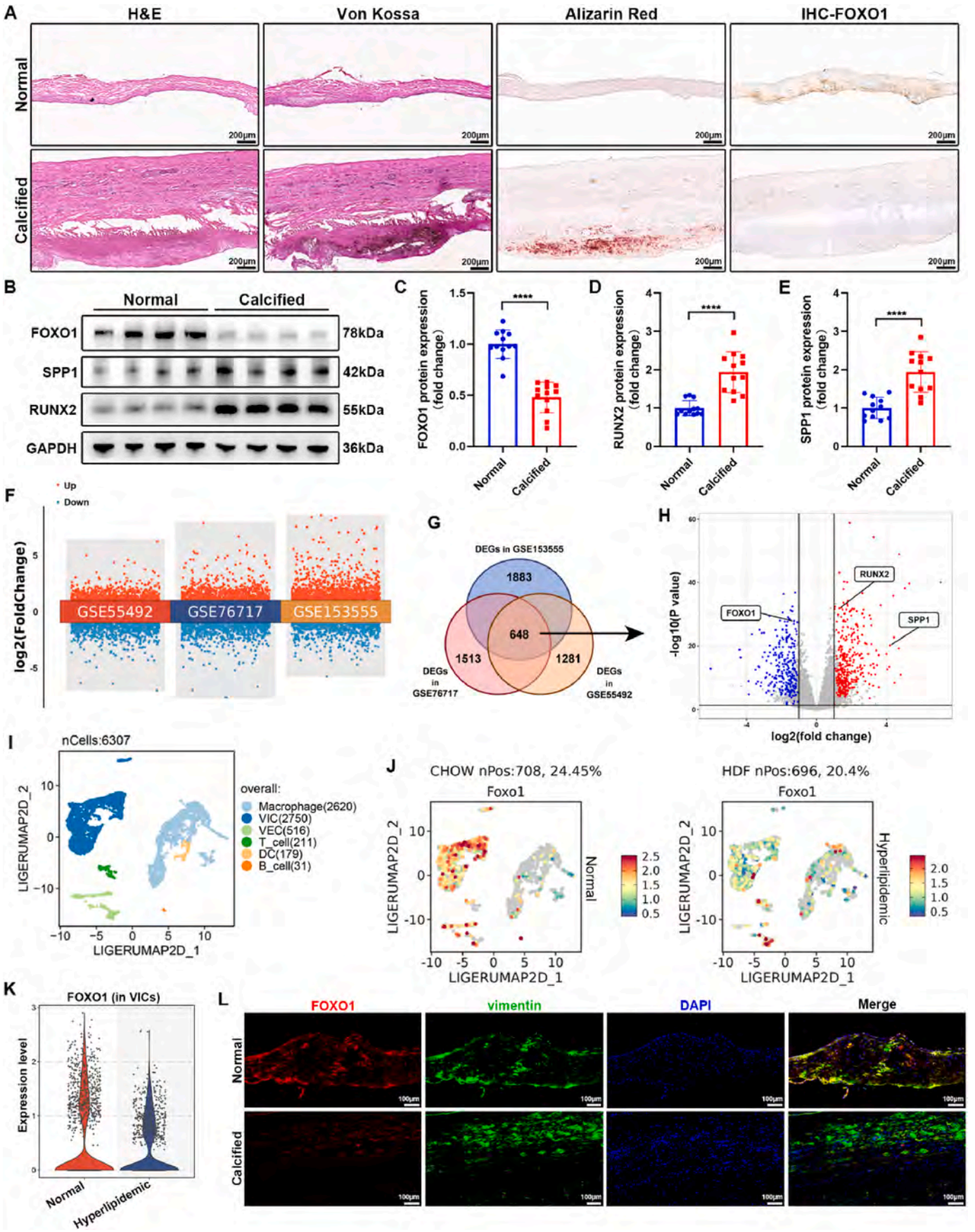

(caption on next page)

Fig. 1. FOXO1 is down-regulated in VICs of human calcific aortic valves. (A) H&E, Von Kossa, Alizarin Red staining and Immumohistochemical staining of FOXO1 in aortic valves, scale bar: 200 μm. (B–E) Western blot of FOXO1, RUNX2 and SPP1 expression in aortic valves (n = 12 independent human aortic valves per group). (F) Differential gene expression analysis showing up- and down-regulated genes in calcified valves compared to normal valves across three bulk RNA-seq datasets. (G) Venn diagram comparing the DEGs between three bulk RNA-seq datasets. (H) Volcano plot of the 648 common DEGs which were marked by blue or red dots. (I) Reduction dimplot of mice aortic valves scRNA-seq. (J) Featureplot revealed a remarkable down-regulation of FOXO1 in aortic valves from mice with hyperlipidemia. (K) Volcano plot showed that FOXO1 represented a significant down-regulation among transcriptional factors in VIC of hyperlipidemia mice. (L) Immunofluorescence staining of FOXO1 and vimentin in aortic valves, scale bar: 100 μm. Values are mean ± SD. Statistical differences were determined by Mann-Whitney test (D) and two-tailed unpaired Student's t-test (C and E). *p < 0.05, **p < 0.01, ***p < 0.001, ****p < 0.0001.

to transfection. The cells were then transfected with individual siRNAs using Lipofectamine 3000 (Thermo Fisher Scientific, L3000075) according to the manufacturer's instructions, then the cells were used for further experiments following cultured for an additional 48 h.

2.17. Antibodies and reagents

The following antibodies were used for western blotting, immunohistochemistry and immunofluorescence: FOXO1 (CST, 2880), p-FOXO1 (CST, 9461), AKT (CST, 4691), p-AKT (CST, 4060), RUNX2 (CST, 8486), SPP1 (Proteintech, 22952-1-AP), GAPDH (Proteintech, 60004-1-Ig), vimentin (Proteintech, 60330-1-Ig), Flag-tag (Proteintech, 66008-4-Ig), His-tag (Proteintech, 10001-0-AP), HA-tag (Proteintech, 51064-2-AP), Myc-tag (Proteintech, 16286-1-AP), SMURF2 (Abclonal, A2278), goat anti-rabbit IgG (ab150077, 1:200 dilution), goat anti-mouse IgG (ab150115, 1:200 dilution).

The following antibodies were used in IP: FOXO1 (Proteintech, 66457-1-Ig), RUNX2 (Santa Cruz, sc-390715), Flag-tag (Proteintech, 66008-4-Ig), His-tag (Proteintech, 66005-1-Ig), HA-tag (Proteintech, 51064-2-AP), HA-tag (Proteintech, 51064-2-AP). MK2206 (Selleck, S1078) was used at a concentration of 1 μM for 24 h. AS1842856 (Selleck, S8222) was used at a concentration of 3 μM for 24 h. MG132 (Selleck, S2619) was used at a concentration of 2.5 μM for 8 h. Cycloheximide (Selleck, S7418) was used at a concentration of 50 μg/μL in different time points within 8 h.

2.18. Statistics analysis

Experimental data were analysed using GraphPad Prism 8 (GraphPad Software, Inc., CA, USA). Values are presented as mean ± standard deviation (SD). The Shapiro-Wilk normality test was used to confirm the normality of the data. If the data passed the normality test (alpha = 0.05), then a parametric test, such as unpaired *t*-test or ordinary one-way ANOVA was used. If the data did not pass the normality test, a non-parametric test was used (Mann-Whitney test). Statistical significance was set at $P < 0.05$.

3. Results

3.1. FOXO1 is down-regulated in VICs of human calcific aortic valves

To investigate the expression of FOXO1 in human calcific aortic valves, normal aortic valves and calcified aortic valves were collected from cardiac transplantation and aortic valve replacement surgery (see Table S1 for patient characteristics). The presence of calcium deposition was confirmed through Von Kossa staining and Alizarin Red staining (Fig. 1A). Meanwhile, FOXO1 was found significantly down-regulated in calcified aortic valves compared with normal valves through immumohistochemical staining (Fig. 1A) and immunoblotting, in contrast to the osteogenic markers RUNX2 and SPP1 (Fig. 1B–E).

To further investigate the changes of FOXO1 expression in CAVD, the bulk RNA-seq datasets GSE76718, GSE153555 and GSE148219 were obtained from the NCBI GEO database (Fig. 1F). There were 648 common differentially expressed genes (DEGs) identified by the interaction of these three datasets (Fig. 1G), in which FOXO1, RUNX2 and SPP1 all showed high significance (Fig. 1H) and conformity with the experimental results (Fig. 1A–E). Interestingly, FOXO1 has a strong negative correlation with RUNX2 (Figure S1). Furthermore, based on the valve scRNA-seq data of hyperlipidemia mice previously reported [21], all cells in valves were divided into 6 subsets including VICs, VECs, Marcrophage, DC, T cell, and B cell (Fig. 1I), and FOXO1 was significantly down-regulated in the VICs and the myofibroblast subsets highly similar to the VICs in the hyperlipidemias compared with the control group (Fig. 1J and K). Subsequently, the result was confirmed by immunofluorescence staining of FOXO1 and vimentin (Fig. 1L), which is a surface marker for VICs. These data suggest that the changes of FOXO1 in VICs may play a role in the development CAVD.

3.2. FOXO1 inhibits osteogenic differentiation of VICs

To investigate whether FOXO1 participate in the osteogenic differentiation of VICs, the primary VICs was isolated and cultured (see Figure S2 for cell phenotyping) in osteogenic medium (OM). Over the course of osteogenic induction, the expression of FOXO1 showed a gradual decreased and on the contrary, RUNX2 and SPP1 gradually increased (Fig. 2A–D). This suggests that FOXO1 may be involved in the osteogenic differentiation of VICs. To further evaluate the effects of FOXO1 on the osteogenic differentiation of VICs, we treated VICs with adenovirus (Ad-FOXO1) or siRNA (siFOXO1) for 48 h to overexpress or silence FOXO1, followed by OM induction for 3days for immunoblotting and 21 days for Alizarin red staining. The results showed that FOXO1 overexpression (Figure S3) counteracted the increased RUNX2 and SPP1 (Fig. 2E–H) and calcium deposition (Fig. 2I–K) derived by osteogenic induction. Conversely, the silencing of FOXO1 (Figure S4) yielded contrasting effects (Fig. 2L-R). These results indicated that FOXO1 prevented the osteogenic differentiation of VICs.

3.3. FOXO1 participates in VICs osteogenic differentiation mediated by AKT pathway

The AKT/FOXO1 axis has been found play an important role in a variety of disease processes [22]. In particular, AKT pathway has been reported to be associated with CAVD [23–26], but its relationship with FOXO1 in CAVD remains unclear. We performed gene set enrichment analysis (GSEA) using the DEGs in bulk RNA-seq mentioned above and found that PI3K/AKT signaling pathway was significantly activated in calcified valve tissue (Fig. 3A). Subsequently, immunofluorescence staining and immunoblotting confirmed that AKT phosphorylation was increased in calcified aortic valves (Fig. 3B–D). Meanwhile, in vitro, we found that the phosphorylation levels of AKT and FOXO1 significantly increased in the osteogenic induction (Fig. 3E–G). In order to examine the impact of the AKT pathway on osteogenic differentiation of VICs, we administered the AKT inhibitor MK2206 to VICs for 24 h prior to osteogenic induction for 3 days. Immunoblotting showed that MK2206 effectively decreased the phosphorylation levels of both AKT and FOXO1, and reversed VICs osteogenic differentiation induced by osteogenic induction (Fig. 3H-L and Figure S5). Additionally, MK2206 significantly reduced the VICs calcium deposition in vitro (Fig. 3M), suggesting that osteogenic induction facilitates osteogenic differentiation through the activation of phosphorylated AKT and FOXO1 in VICs.

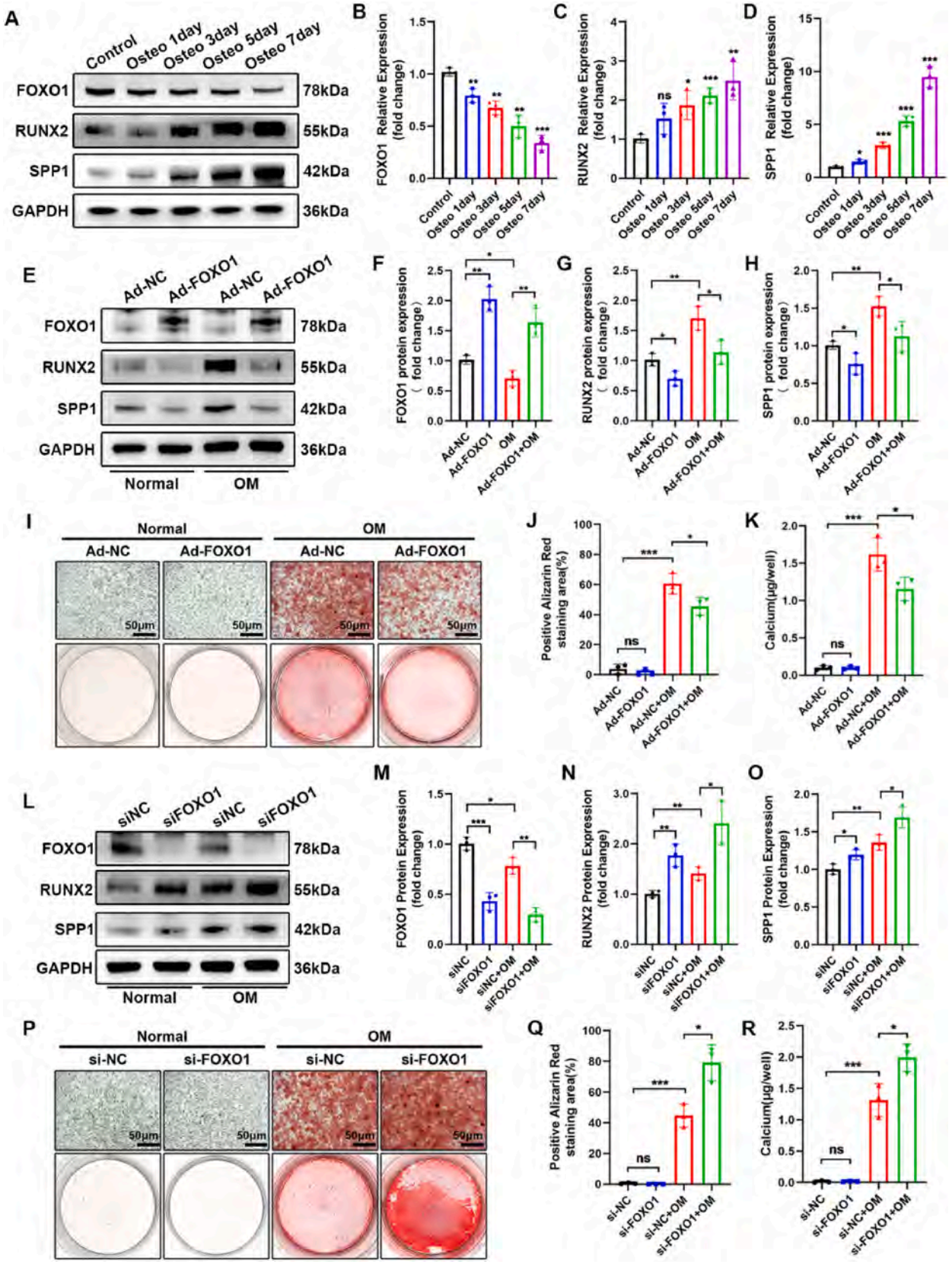

Fig. 2. FOXO1 inhibits osteogenic differentiation of VICs. (A–D) Western blot analysis of protein levels in VICs with osteogenic medium at different time points (days 0, 1, 3, 5, 7, n = 3 independent experiments). (E–H) Western blot analysis of FOXO1, RUNX2 and SPP1 in VICs with FOXO1 overexpression and osteogenic medium (n = 3 independent experiments). Alizarin red staining of calcium deposition (I–J) and calcium content (K) in VICs overexpressing FOXO1 (n = 3 independent experiments). (L–O) Western blot analysis of FOXO1, RUNX2 and SPP1 in VICs following FOXO1 silencing (n = 3 independent experiments). Alizarin red staining of calcium deposition (P–Q) and calcium content (R) in VICs following FOXO1 silencing (n = 3 independent experiments). Scale bar: 50 μm. Values are mean ± SD. All statistical differences were determined using two-tailed unpaired Student's t-test. *p < 0.05, **p < 0.01, ***p < 0.001, ****p < 0.0001.

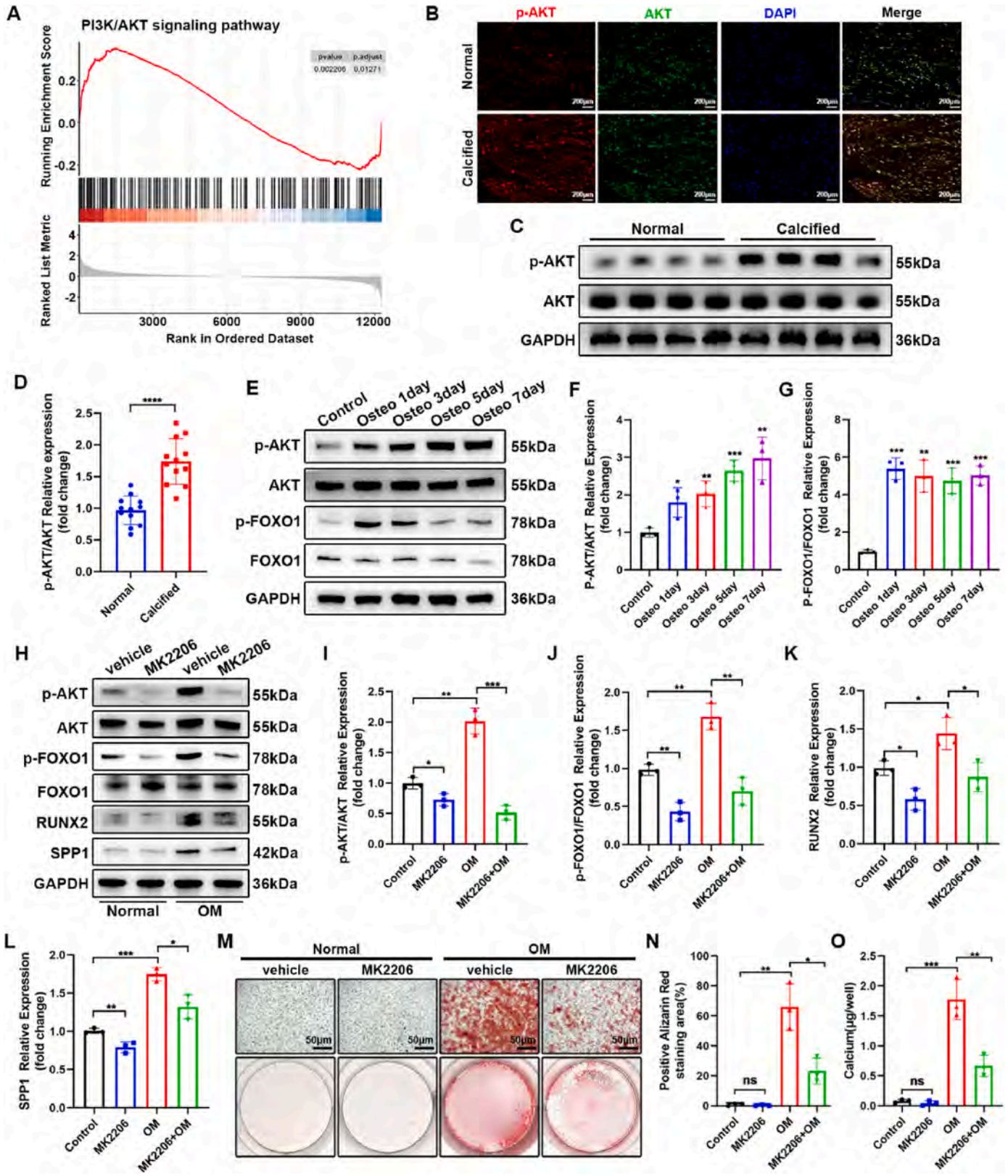

Fig. 3. FOXO1 participates in VICs osteogenic differentiation mediated by AKT pathway. (A) GSEA of bulk RNA-seq showed an up-regulation of PI3K/AKT pathway. (B) Immunofluorescence staining of p-AKT and AKT in aortic valves, scale bar: 200 μm. (C–D) Western blot analysis of p-AKT and AKT expression in aortic valves. (n = 12 independent human aortic valves per group). (E–G) Western blot analysis of protein levels in VICs with osteogenic medium at different time points (days 0, 1, 3, 5, 7, n = 3 independent experiments). (H–L) Western blot analysis of protein levels in VICs with MK2206 and osteogenic medium (n = 3 independent experiments). Alizarin red staining of calcium deposition (M − N) and calcium content (O) in VICs with MK2206 and osteogenic medium (n = 3 independent experiments). Scale bar: 50 μm. Values are mean ± SD. Statistical differences were determined using Benjamini-Hochberg (BH)-procedure (Multiple comparison test) (A) and two-tailed unpaired Student's t-test (D, F, G, I-L, N and O). *p < 0.05, **p < 0.01, ***p < 0.001, ****p < 0.0001.

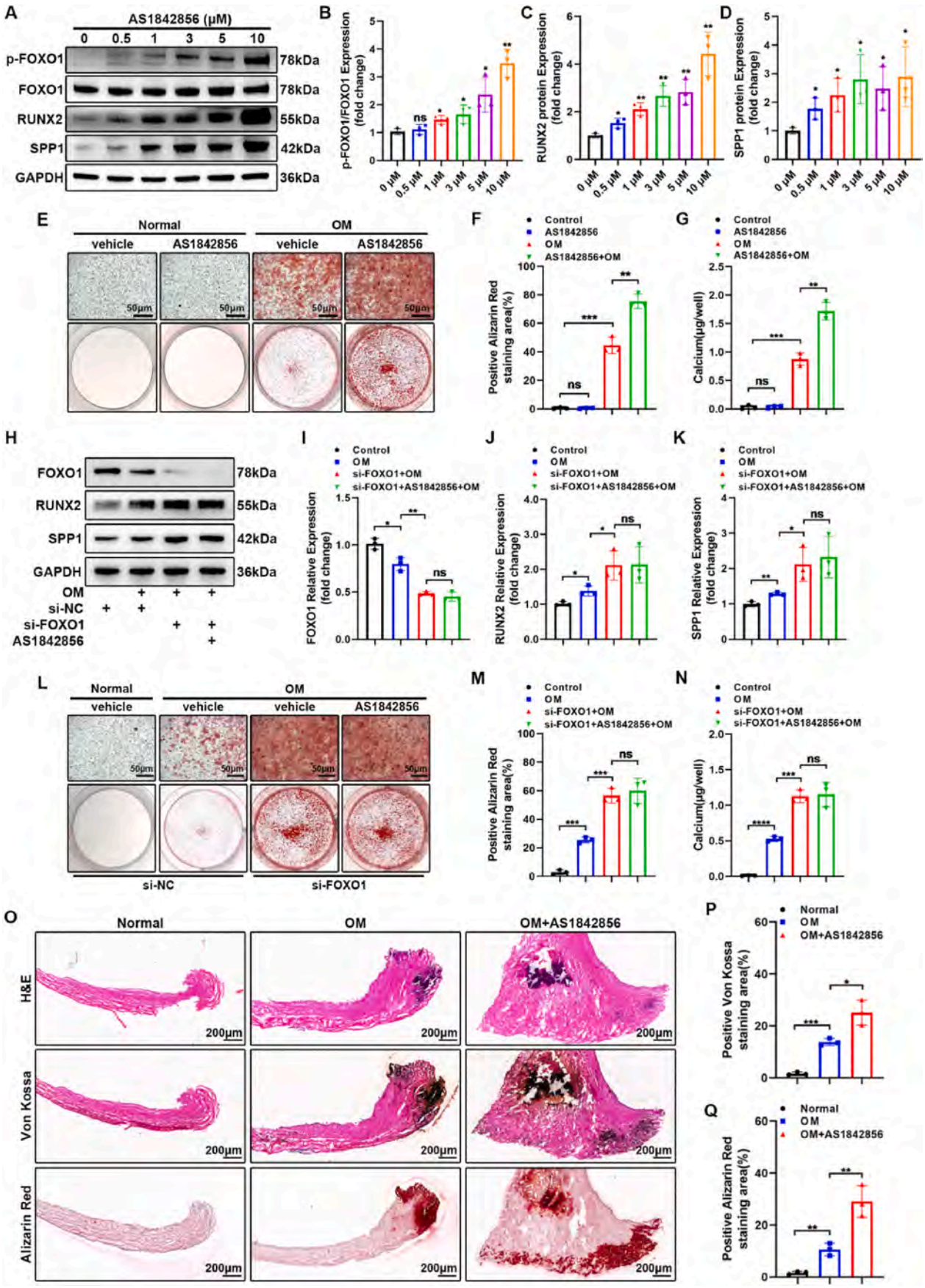

(caption on next page)

Fig. 4. FOXO1 inhibitor AS1842856 promotes osteogenic differentiation of VICs by promoting FOXO1 phosphorylation. (A–D) Western blot analysis of protein levels in VICs with AS1842856 in 0, 0.5, 1, 3, 5 and 10 μM (n = 3 independent experiments). Alizarin red staining of calcium deposition (E–F) and calcium content (G) in VICs with AS1842856 and osteogenic medium (n = 3 independent experiments). (H–K) Western blot analysis of protein levels in VICs with FOXO1 silencing, AS1842856 and osteogenic medium (n = 3 independent experiments). Alizarin red staining of calcium deposition (L–M) and calcium content (N) in VICs with FOXO1 silencing, AS1842856 and osteogenic medium (n = 3 independent experiments). (O–Q) H&E, Von Kossa and Alizarin Red staining of aortic valves treated with AS1842856 and osteogenic medium in vitro (n = 3 independent experiments). scale bar: 200 μm. Values are mean ± SD. All statistical differences were determined using two-tailed unpaired Student's t-test. *p < 0.05, **p < 0.01, ***p < 0.001, ****p < 0.0001.

3.4. FOXO1 inhibitor AS1842856 promotes osteogenic differentiation of VICs by promoting FOXO1 phosphorylation

In order to examine the impact of FOXO1 phosphorylation on the osteogenic differentiation of VICs, we treated VICs with AS1842856, a FOXO1 inhibitor, at varying concentrations for 24 h. The results showed that AS1842856 promoted FOXO1 phosphorylation, and simultaneously, RUNX2 and SPP1 gradually increased (Fig. 4A–D). In addition, AS1842856 promoted the formation of calcium deposition in VICs induced by osteogenic medium (Fig. 4E–G). However, the procalcification effects of AS1842856 were eliminated when FOXO1 expression was silenced (Fig. 4H-N), which indicated that the procalcific effect of AS1842856 is reliant on the presence of FOXO1. Furthermore, an ex-vivo valves osteogenic differentiation model was performed. Normal human aortic valves were cut into small pieces and cultured in osteogenic medium for 2 months with or without AS1842856. H&E, Von kossa, Alizarin Red staining showed that AS1842856 could significantly aggravate the calcium deposition in the valves (Fig. 4O-Q). These results indicated that FOXO1 inhibition could aggravate the calcification of VICs and aortic valve in vitro.

3.5. FOXO1 inhibition aggravates aortic valve calcification in vivo

In order to investigate the involvement of FOXO1 in the process of aortic valve calcification in vivo, we administered either vehicle or AS1842856 to *Apoe*$^{-/-}$ mice. There was no significant difference of aortic valve peak transvalvular jet velocity and mean transvalvular pressure gradient between the two groups of mice before the high cholesterol diet feeding (Fig. 5A–C). Following a 24-week period of consuming a high cholesterol diet, the efficiency of AS1842856 in the aortic valves was validated by immunofluorescence staining of aortic valves. The results showed that phosphorylation of Foxo1 was significantly up-regulated (Figure S6), while Foxo1 expression was slightly down-regulated in the aortic valve leaflets (Figure S7). The down-regulation of Foxo1 may be related with the nuclear efflux, ubiquitination and degradation of Foxo1 after phosphorylation [27]. The mice in the AS1842856 group exhibited noteworthy elevations in peak transvalvular jet velocity and mean transvalvular pressure gradient (Fig. 5A–C). There were no substantial disparities observed in left ventricular (LV) diameters or hemodynamic parameters between the groups (Table S3). Additionally, H&E, Von Kossa, Alizarin Red and Masson staining showed that the aortic valve leaflet of AS1842856 group mice demonstrated elevated levels of calcium deposition and collagen formation (Fig. 5D–K). And immunofluorescence staining showed that Runx2 significantly up-regulated in AS1842856 group mice (Fig. 5L-M). These results further suggested that FOXO1 inhibition could aggravate aortic valve calcification in vivo.

3.6. FOXO1 interacts with RUNX2 and promotes its ubiquitination and degradation

There are several clues as to the mechanism by which FOXO1 is involved in valve calcification. A previous study reported that FOXO1 could bind to RUNX2 and impede its transcriptional activity [14]. However, this does not provide a comprehensive explanation for the down-regulation of RUNX2 mediated by FOXO1 in VICs. Another study previously reported that the knockdown of FOXO1 resulted in the inhibition of RUNX2 ubiquitination and the promotion of calcification in vascular smooth muscle cells (VSMCs) [28]. This may explain the reduction of RUNX2 mediated by FOXO1. Nevertheless, the interaction between FOXO1 and RUNX2 in VICs remains unclear.

To investigate the interaction between FOXO1 and RUNX2, VICs were simultaneously treated with Flag-tagged FOXO1 and His-tagged RUNX2 for 48 h. Coimmunoprecipitation (co-IP) analysis demonstrated that exogenously overexpressed Flag-FOXO1 could bind to His-RUNX2 in VICs (Fig. 6A). The interaction between endogenous FOXO1 and RUNX2 was also confirmed in VICs (Fig. 6B). Overexpression of FOXO1 resulted in the down-regulation of RUNX2, which was mitigated by the 26S proteasome inhibitor MG132 (Fig. 6C–E). Furthermore, FOXO1 overexpression reduced the half-life of RUNX2 (Fig. 6F and G) and increased RUNX2 ubiquitination in VICs (Fig. 6H). These results confirmed that FOXO1 could interact with RUNX2 and promote its ubiquitination and degradation. In addition, interestingly, we found that the ubiquitination of RUNX2 and interaction between FOXO1 and RUNX2 could be weakened by AS1842856 (Fig. 6H).

The phosphorylation of FOXO1 has been found to promote its exclusion from the nucleus [14,28]. In light of this, we formulated a hypothesis suggesting that the regulatory effect of AS1842856 on RUNX2 ubiquitination may be linked to the nuclear exclusion of FOXO1. To confirm the hypothesis, we utilized the Nuclear and Cytoplasmic Protein Extraction Kit to extract the protein from VICs treated with AS1842856. Subsequent Western blot analysis revealed a decrease in the expression of FOXO1 in the nucleus, accompanied by an increase in its expression in the cytoplasm and however, the overall expression level of FOXO1 did not exhibit a significant change (Fig. 6I). Meanwhile, the increased RUNX2 was mainly present in the nucleus of VICs, and it was almost absent in the cytoplasm (Fig. 6I). In addition, immunoprecipitation of FOXO1 after treatment of VICs with AS1842856 and MK2206 showed that RUNX2 was decreased in the AS1842856 group and increased in the MK2206 group, further demonstrating that AKT inhibition enhances the binding of FOXO1 to RUNX2. However, the binding of FOXO1 to RUNX2 was reduced after phosphorylation, resulting in the release of RUNX2.(Figure S8). Further confirmation of the co-localization of FOXO1 and RUNX2, as well as nuclear exclusion of FOXO1 was obtained through immunofluorescence staining of VICs (Fig. 6J).

3.7. FOXO1 promotes SMURF2-mediated RUNX2 ubiquitination in VICs

The above results indicate that FOXO1 facilitate the ubiquitination of RUNX2, but FOXO1 itself does not function as an E3 ubiquitin ligase. We hypothesized that FOXO1, as a transcription factor, may mediate the expression of some E3 ubiquitin ligases of RUNX2, thereby promoting the ubiquitination of RUNX2. In order to obtain the possible E3 ubiquitin ligase of RUNX2, we employed UbiBrowser 2.0 to perform the prediction. We identified 26 possible E3 ubiquitin ligases of RUNX2, in which 20 were predicted and 6 had been validated (Fig. 7A). We first conducted validation and screening procedures on the six validated E3 ubiquitin ligases of RUNX2. qRT-PCR analysis revealed that only SMURF2 exhibited significantly down-regulation after VICs were treated with AS1842856 (Fig. 7B). Subsequently, qRT-PCR and Western blot analysis demonstrated that the down-regulation of SMURF2 induced by osteogenic medium could be reversed by FOXO1 overexpression, and AS1842856 was able to further reverse the effect of FOXO1 overexpression (Fig. 7C–E). These results suggest that SMURF2 expression is regulated by FOXO1. However, whether SMURF2 can mediate RUNX2

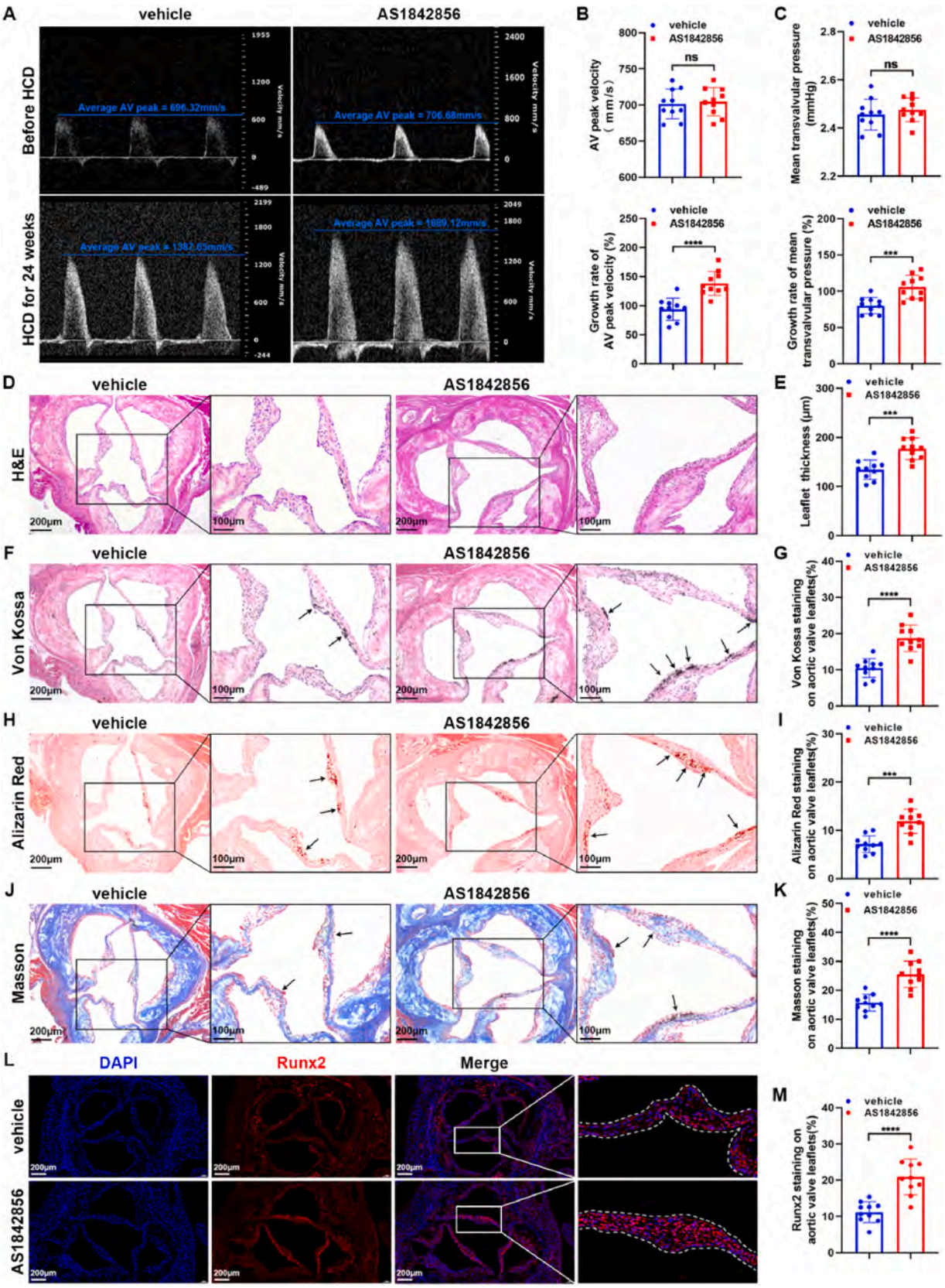

Fig. 5. FOXO1 inhibition aggravates aortic valve calcification in vivo. Echocardiographic date of peak transvalvular jet velocity (A–B) and mean transvalvular pressure gradient (C) in *Apoe*$^{-/-}$ mice treated with or without AS1842856. H&E staining (D–E), Von Kossa staining (F–G), Alizarin Red staining (H–I) and Masson's trichrome staining (J–K) of aortic valve leaflets from *Apoe*$^{-/-}$ mice treated with or without AS1842856. scale bar: 200 μm or 100 μm. (L–M) Immunofluorescence staining of Runx2 (red) in aortic valves. DAPI was used for nuclear counterstaining (blue). scale bar: 200 μm. Values are the mean ± SD. All statistical differences were determined using two-tailed unpaired Student's t-test. *p < 0.05, **p < 0.01, ***p < 0.001, ****p < 0.0001. n = 10 independent mice per group.

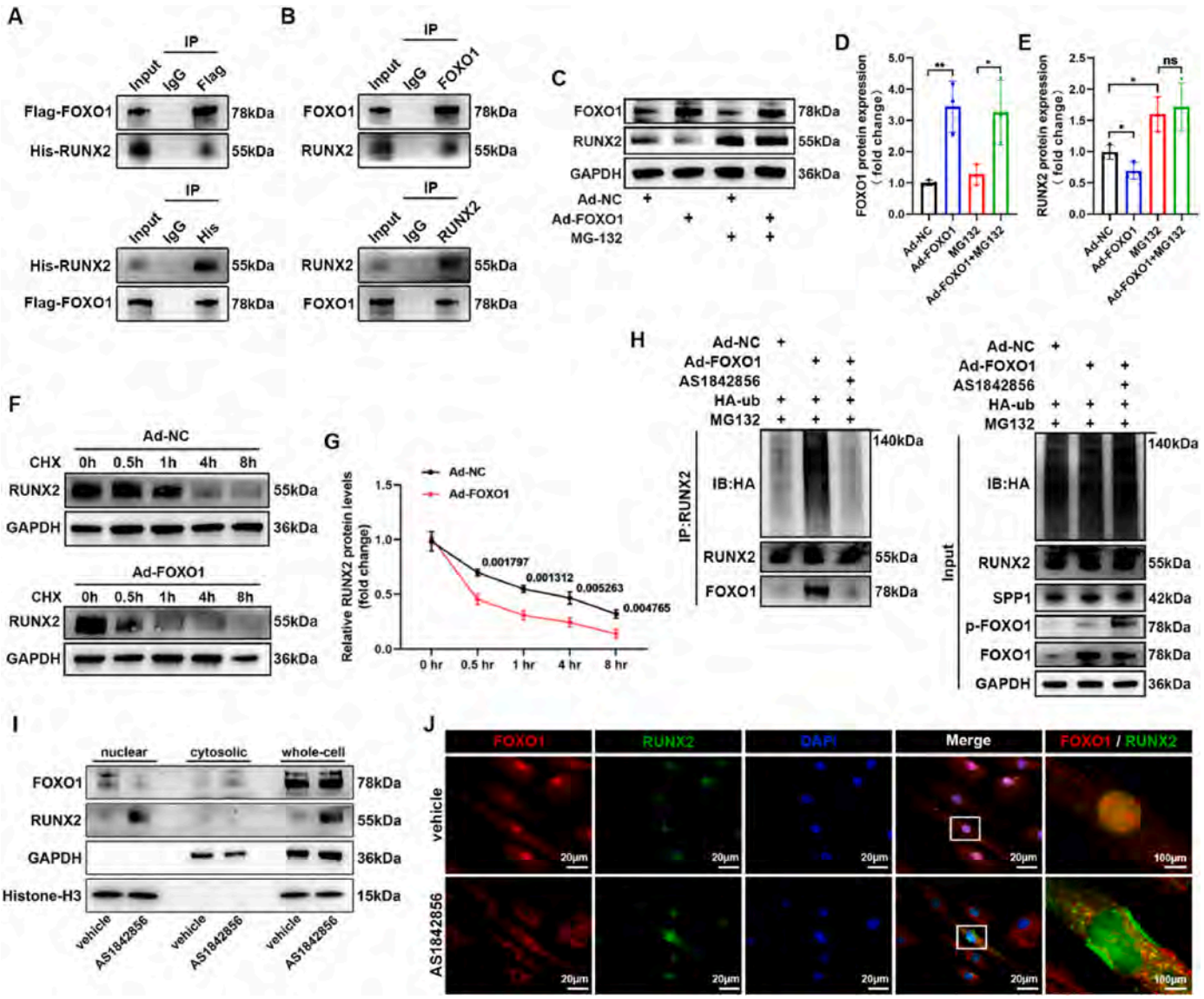

Fig. 6. FOXO1 interacts with RUNX2 and promotes its ubiquitination and degradation. (A) Co-immunoprecipitation (co-IP) to detect the interaction between Flag-tagged FOXO1 (Flag-FOXO1) and His-tagged RUNX2 (His-RUNX2). (B) Co-immunoprecipitation (co-IP) to detect the interaction between endogenous FOXO1 and RUNX2. (C–E) VICs were treated with Ad-NC or Ad-FOXO1 for 48 h. Before immunoblotting, cells were treated with the 26S proteasome inhibitor MG132 for 8 h (n = 3 independent experiments). (F–G) Western blot analysis of RUNX2 and GAPDH in VICs treated with Ad-Control or Ad-FOXO1 for 48 h, then treated with cycloheximide (CHX) for 0, 0.5, 1, 4 and 8 h (n = 3 independent experiments). (H) Co-IP to detect RUNX2 ubiquitination. VICs were treated with Ad-FOXO1 and AS1842856 for 48 h, then treated with MG132 for 8 h. The protein lysates were immunoprecipitated with an anti-RUNX2 antibody and immunoblotted with the indicated antibodies. (I) Western blot analysis of FOXO1 and RUNX2 in the nuclear, cytosolic and whole-cell of VICs treated with AS1842856. (J) Immunofluorescence staining of FOXO1 (Red) and RUNX2 (Green) in VICs treated with AS1842856. DAPI was used for nuclear counterstaining (blue). Scale bar: 20 μm. Values are mean ± SD. Statistical differences were determined using two-tailed unpaired Student's t-test (D and E) and Two-way ANOVA followed by *Bonferroni post hoc* test (G). *p < 0.05, **p < 0.01, ***p < 0.001, ****p < 0.0001.

ubiquitination in VICs remains unknown.

To confirm the interaction between SMURF2 and RUNX2, VICs were simultaneously treated with Myc-tagged SMURF2 and His-tagged RUNX2. Co-IP analysis demonstrated that exogenously overexpressed Myc-SMURF2 was capable of binding to His-RUNX2 in VICs (Fig. 7F). The interaction between endogenous SMURF2 and RUNX2 was also confirmed in VICs (Fig. 7G). Overexpression of SMURF2 (Figure S9) resulted in down-regulation of RUNX2, which was mitigated by MG132 (Fig. 7H). Furthermore, SMURF2 overexpression led to a shortened half-life of RUNX2 and increased ubiquitination of RUNX2 in VICs (Fig. 7K-M). In addition, we found that SMURF2 silencing (Figure S10) significantly attenuated the FOXO1-mediated ubiquitination of RUNX2 (Figure S11), suggesting that the regulatory effect of FOXO1 on RUNX2 ubiquitination is SMURF2-dependent. Further confirmation of the co-localization of SMURF2 and RUNX2 was obtained through immunofluorescence staining (Fig. 7N). Besides, Smurf2 down-regulation in calcified aortic valves was confirmed by immunofluorescence staining from *Apoe*$^{-/-}$ mice treated with AS1842856 (Fig. 7O-P).

3.8. FOXO1 inhibits the osteogenic differentiation of VICs by up-regulating SMURF2

To further validate the role of SMURF2 in the process of VICs osteogenic differentiation, rescue experiments were conducted. The results showed that overexpression of SMURF2 (Figure S9) prevented the promoting calcific effects of AS1842856 (Fig. 8A–G), while silencing of

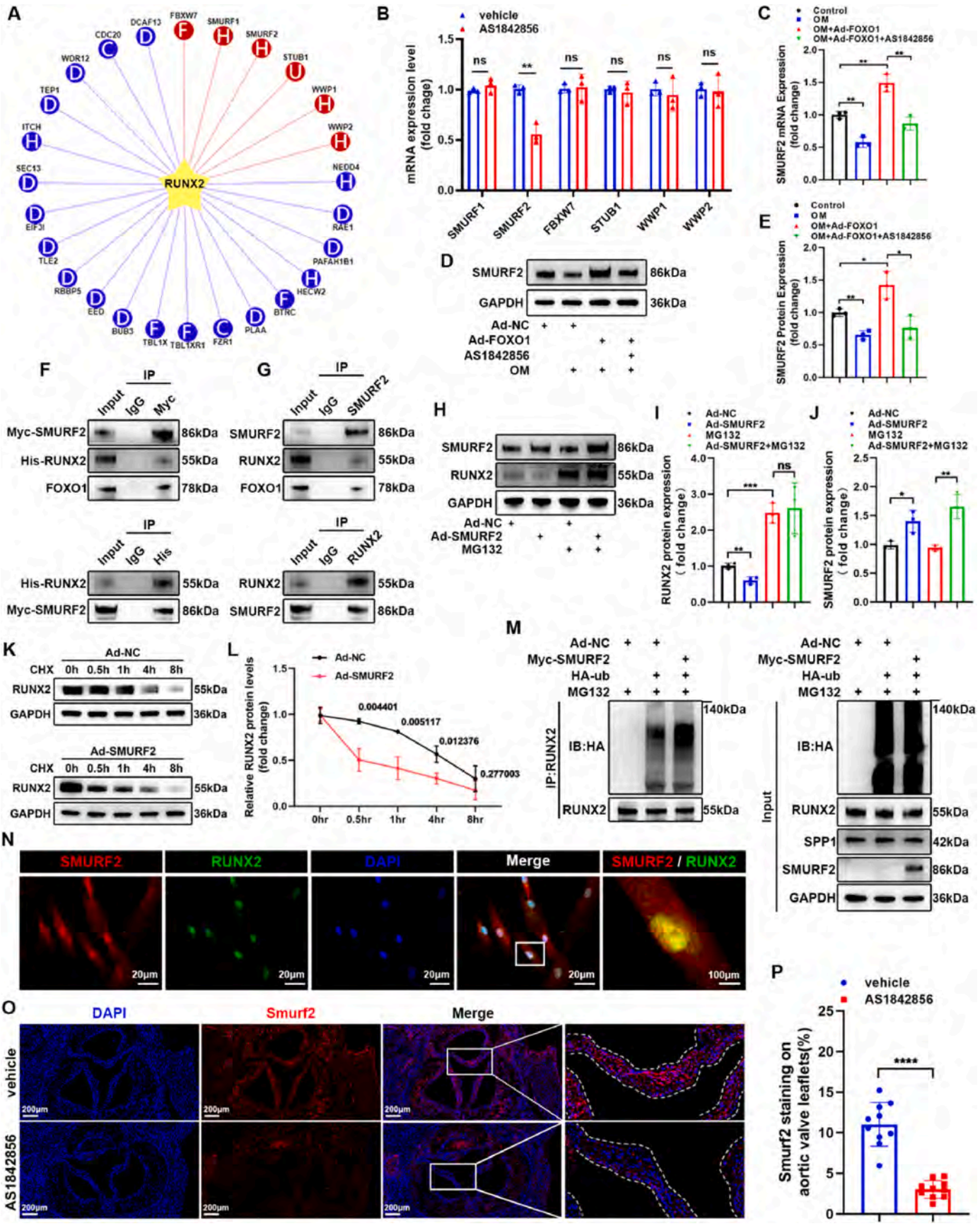

(caption on next page)

Fig. 7. FOXO1 promotes SMURF2-mediated RUNX2 ubiquitination in VICs. (A) E3 ubiquitin ligases of SMURF2 predicted by the UbiBrowser 2.0. (B) qRT-PCR analysis of the predicted E3 ubiquitin ligases of RUNX2 in VICs treated with AS1842856 (n = 3 independent experiments). (C–E) qRT-PCR and Western blot analysis of SMURF2 in VICs treated with FOXO1 overexpression, AS1842856 and osteogenic medium (n = 3 independent experiments). (F) Co-immunoprecipitation (co-IP) to detect the interaction between Myc-tagged SMURF2 (Myc-SMURF2) and His-tagged RUNX2 (His-RUNX2). (G) Co-immunoprecipitation (co-IP) to detect the interaction between endogenous SMERF2 and RUNX2. (H–J) Western blot analysis of VICs treated with FOXO1 overexpression and MG132 (n = 3 independent experiments). (K–L) Western blot analysis of RUNX2 and GAPDH in VICs treated with Ad-Control or Ad-FOXO1 for 48 h, then treated with CHX for 0, 0.5, 1, 4 and 8 h (n = 3 independent experiments). (M) Co-IP to detect RUNX2 ubiquitination. The protein lysates were immunoprecipitated with an anti-RUNX2 antibody and immunoblotted with the indicated antibodies. (N) Immunofluorescence staining of SMURF2 (Red) and RUNX2 (Green) in VICs. DAPI was used for nuclear counterstaining (blue). Scale bar: 20 μm. (O–P) Immunofluorescence staining of Smurf2 (red) in aortic valves (n = 10 independent mice per group). DAPI was used for nuclear counterstaining (blue). scale bar: 200 μm. Values are mean ± SD. Statistical differences were determined using two-tailed unpaired Student's t-test (B, D, E, I and J) and Two-way ANOVA followed by *Bonferroni post hoc* test (L). *p < 0.05, **p < 0.01, ***p < 0.001, ****p < 0.0001.

SMURF2 reversed the alleviating calcification effects of FOXO1 (Fig. 8H-N). Furthermore, the alleviating calcification effect was further enhanced by simultaneous overexpression of FOXO1 and SMURF2 (Fig. 8O-U).

4. Discussion

With the trend of global population aging, the prevalence of CAVD keeps elevating [29], but there has been a lack of effective drug therapy [30]. CAVD is a complex ailment characterized by considerable heterogeneity [31]. Its pathogenesis encompasses endothelial damage, lipoprotein accumulation, inflammation, and osteogenic differentiation of VICs [32]. FOXO1, as a classical downstream gene of PI3K/AKT signaling pathway, has been found play a role in cardiovascular diseases like atherosclerosis and vascular calcification [32]. But the relationship between FOXO1 and CAVD still unclear. This study presents novel findings, demonstrating that FOXO1 mitigates aortic valve calcification by means of SMURF2-mediated ubiquitination and degradation of RUNX2 (Graphical Abstract).

First of all, we obtained normal and calcified aortic valves. In this process, the distinction between normal and calcified valves can be difficult since some parts may be sclerotic. This kind of valves was predominantly fibrotic and needs to be excluded based on the presence or absence of hyperechogenic calcification on echocardiography, otherwise it may affect the stability of the results, as we only focused on calcified valves. We found that FOXO1 was significantly down-regulated in calcified aortic valves compared with normal ones. This result was consistent with the bulk RNA-seq data from GEO database. Furthermore, we analysed the scRNA-seq data from the aortic valves of mice (GSE180278) and found that FOXO1 significantly down-regulated in VICs. During the progression of CAVD, VICs undergo osteogenic differentiation, leading to the formation of calcium salt deposits and subsequent valve calcification [33]. That's why we next focused on exploring the relationship between FOXO1 and calcification in VICs.

While the functions of FOXO1 in osteogenesis had been reported previously [28,34], its role in CAVD remains uncertain. Our investigation demonstrated that the overexpression of FOXO1 reduced the expression of osteogenic markers RUNX2 and SPP1, as well as calcium deposition in VICs treated with an osteogenic medium. Conversely, the silencing of FOXO1 exacerbated osteogenic differentiation. These findings suggest that FOXO1 exerts an anti-calcification effect in VICs, although the underlying mechanism remains to be elucidated.

PI3K/AKT pathway, as a classical upstream regulator of FOXO1, has been reported to be associated with the progress of CAVD [23]. Elena Aikawa et al. found that PI3K/AKT signaling pathway was significantly enriched in the fibrosa of calcified aortic valve [35]. However, it was unclear whether FOXO1 is involved in the process of VICs osteogenic differentiation mediated by AKT. In the present study, we demonstrated that the phosphorylation of AKT was up-regulated in calcified aortic valves compared to normal ones. And in vitro, the phosphorylation of both AKT and FOXO1 were increased in VICs induced by osteogenic medium, which was reversed by AKT inhibitor MK2206, and the osteogenic differentiation and calcium deposition of VICs were reduced either. These results indicated that AKT activated by osteogenic induction promoted the osteogenic differentiation of VICs, during which the phosphorylation of FOXO1 was activated by AKT. However, the role of FOXO1 phosphorylation in osteogenic differentiation of VICs remains unclear.

AS1842856 is a specific inhibitor of FOXO1, discovered by Takeyuki Nagashima et al. [36]. Over the years, researchers have had different opinions about the effect of AS1842856 on FOXO1. In the present study, we demonstrated that AS1842856 promoted the Ser256 phosphorylation of FOXO1 in a dose-dependent manner. Besides, AS1842856 significantly enhanced the expression of RUNX2 and SPP1, as well as the calcium deposition in VICs. Moreover, these effects were abolished upon silencing of FOXO1, which indicated that the function of AS1842856 was dependent on the presence of FOXO1. Subsequently, we performed an ex-vivo osteogenic differentiation model, which confirmed that AS1842856 induced aortic valve calcification in vitro. Then we further confirmed that AS1842856 aggravated the aortic valves calcification in *Apoe*$^{-/-}$ mice. This is the first study to show that FOXO1 inhibition exacerbates aortic valve calcification in vitro an in vivo.

Mechanistically, RUNX2 may be a key regulator of FOXO1 affecting osteogenic differentiation of VICs. There were previous findings indicated that FOXO1 could bind to RUNX2 and inhibit its transcriptional activity [14], and FOXO1 silencing led to a decrease of RUNX2 ubiquitination [28]. But how FOXO1 affects RUNX2 ubiquitination and how this relates to FOXO1 phosphorylation? To figure out the mechanism between them, we first validate the interaction between FOXO1 and RUNX2 through an immunoprecipitation assay. The results demonstrate that FOXO1 facilitated the ubiquitination and degradation of RUNX2, aligning with the previous findings. Intriguingly, the presence of AS1842856 reduced the interaction between FOXO1 and RUNX2, and reversed the FOXO1-mediated promotion of RUNX2 ubiquitination. We postulated that the observed phenomenon may be associated with the nuclear exclusion and phosphorylation of FOXO1. Subsequently, this hypothesis was confirmed through the utilization of western blot analysis and immunofluorescence staining on VICs treated with AS1842856. These results suggested a mechanism that FOXO1 can bind to RUNX2, promote its ubiquitination and degradation, and AS1842856 promote FOXO1 phosphorylation, resulting FOXO1 leave from RUNX2 and excreted out of the nucleus.

E3 ubiquitin ligase is indispensable for protein ubiquitination [37,38]. Considering FOXO1 as a transcription factor in gene expression regulation, rather than an E3 ubiquitin ligase, we proposed that FOXO1 may regulate some E3 ubiquitin ligases of RUNX2, thereby mediating the ubiquitination modification of it. Through the utilization of UbiBrowser 2.0 for prediction and qRT-PCR for screening, our findings suggest that SMURF2 may function as the E3 ubiquitin ligase connecting FOXO1 and RUNX2. It is noteworthy that previous studies have reported SMURF2's role as an E3 ubiquitin ligase for RUNX2, regulating its protein degradation and promoting osteogenic differentiation [39]. This was further confirmed through immunoprecipitation assays conducted in our study. Furthermore, the present study demonstrates that SMURF2 effectively counteracted the impact of FOXO1 on the expression of RUNX2 and the osteogenic differentiation of VICs, thereby suggesting that FOXO1 regulates RUNX2 via SMURF2.

In summary, our findings indicate that FOXO1 was significantly

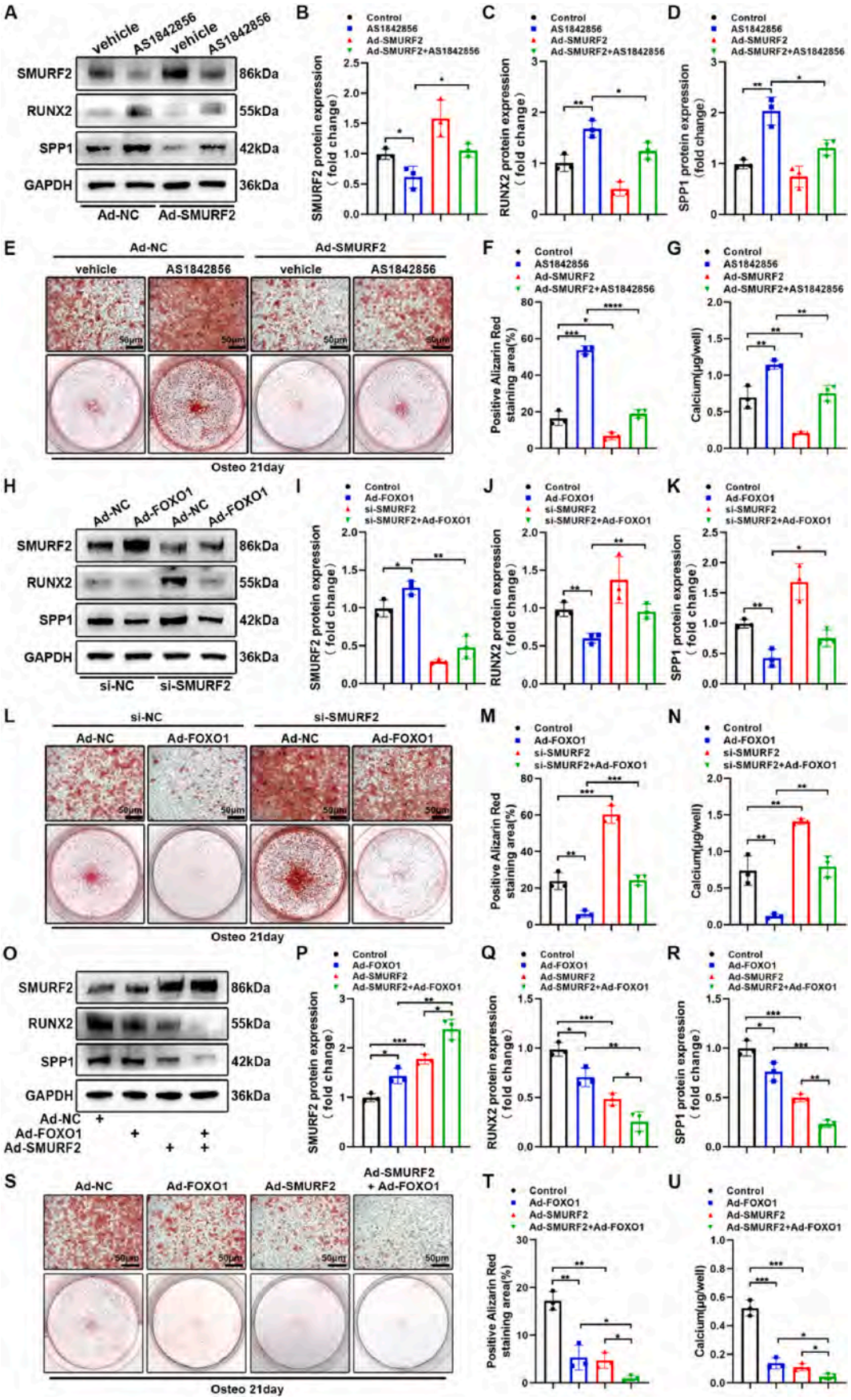

(caption on next page)

Fig. 8. FOXO1 inhibits the osteogenic differentiation of VICs by up-regulating SMURF2. (A–D) Western blot analysis of SMURF2 and osteogenic markers (RUNX2 and SPP1) in VICs with AS1842856 and SMURF2 overexpression (n = 3 independent experiments). Alizarin red staining (E–F) and calcium content (G) in VICs with AS1842856 and SMURF2 overexpression (n = 3 independent experiments). (H–K) Western blot analysis of SMURF2 and osteogenic markers in VICs with FOXO1 overexpression and SMURF2 silencing (n = 3 independent experiments). Alizarin red staining (L–M) and calcium content (N) in VICs with FOXO1 overexpression and SMURF2 silencing (n = 3 independent experiments). (O–R) western blot analysis of SMURF2 and osteogenic markers in VICs with FOXO1 and SMURF2 overexpression (n = 3 independent experiments). Alizarin red staining (S–T) and calcium content (U) in VICs with FOXO1 and SMURF2 overexpression (n = 3 independent experiments). Values are mean ± SD. All statistical differences were determined using two-tailed unpaired Student's t-test. *p < 0.05, **p < 0.01, ***p < 0.001, ****p < 0.0001.

down-regulated in CAVD and played a role in the osteogenic differentiation of VICs by means of the AKT pathway. Moreover, FOXO1 effectively mitigated aortic valve calcification and the osteogenic differentiation of VICs. Mechanistically, FOXO1 exhibited dual functionality by interacting with RUNX2 to suppress its transcriptional activity, while also facilitating the ubiquitination and subsequent degradation of RUNX2 through the up-regulation of SMURF2. This impact of FOXO1 was observed to diminish upon nuclear exclusion, which was induced by osteogenic or drug stimulation.

The present study has several limitations. First, we identified that both mRNA and protein levels of FOXO1 were reduced in calcified aortic valves, but the reason was still unclear. AKT phosphorylation activated by osteogenic induction could promote FOXO1 Ser256 phosphorylation, which may lead to nuclear efflux, ubiquitination and degradation of FOXO1 [27]. However, these can't explain why FOXO1 mRNA down-regulated in CAVD. In addition, FOXO1 has been reported to be down-regulated by type 1 interferons [40] and various of miRNAs [41,42], so it is speculated that the down-regulation of FOXO1 may be at the level of transcription and translation, however the specific mechanism of FOXO1 downregulation in CAVD still needs to be further studied. Second, the osteogenic markers used in the study have certain limitations. SPP1 is one of the osteogenic marker proteins besides the key osteogenic transcription factor RUNX2 [43,44]. In order to mitigate the potential for inaccuracies stemming from the reliance on RUNX2 as the sole osteogenic marker, SPP1, which has shown consistent upregulation with RUNX2 in prior results (Fig. 1H), was included as an additional marker in this study. Although FOXO1 may not have a direct regulatory effect on SPP1, the co-expression of RUNX2 and SPP1 in cardiovascular calcification usually serves as a marker of osteogenic activity, suggesting the differentiation of cells towards an osteogenic phenotype [45,46]. Third, we only investigated the male mice and no female mice. Marie-Annick et al. mentioned that women have less valvular calcification but more fibrosis compared with men [47]. The histopathology of aortic stenosis differs between sexes with a more fibrotic pattern in women and a more calcific pattern in men. Therefore, the male mouse calcification model was used in this study, while the role of FOXO1 in female mice requires further investigated. Finally, we only focused on the targets solely implicated in the calcification process. Actually, the pathogenesis of CAVD is not limited to the valve itself. For example, in chronic kidney disease patient pro-osteogenic pathways are markedly activated leading to CAVD [48–50]. In a network-guided multi-omics study, Aikawa et al. created the first integrated map of human CAVD and established a network of correlations between CAVD and other human diseases [35]. By which, we can expand our vision and investigate CAVD from a more comprehensive perspective in the future.

5. Conclusions

Our study provides new perspectives on the molecular mechanisms regulating RUNX2 in the development of calcific aortic valve disease (CAVD), and highlights the potential clinical importance of FOXO1 and SMURF2 in the evaluation of CAVD.

Funding

This work was supported by the National Key Research and Development Program (no. 2021YFA1101900, 2022YFC2503401), and National Natural Science Foundation of China (no. 82300413, 82200410, 82370379, 81974034, 82170377).

CRediT authorship contribution statement

Chen Jiang: Writing – review & editing, Writing – original draft, Visualization, Investigation, Formal analysis, Data curation, Conceptualization. **Dingyi Yao:** Methodology, Investigation, Conceptualization. **Zongtao Liu:** Resources, Investigation, Formal analysis. **Yidan Zheng:** Visualization, Formal analysis. **Ming Chen:** Visualization, Formal analysis. **Wai Yen Yim:** Visualization, Formal analysis. **Qiang Zheng:** Methodology. **Tailong Zhang:** Data curation. **Lin Fan:** Visualization, Investigation. **Zhengfeng Fan:** Data curation. **Bingchuan Geng:** Methodology. **Rui Tian:** Project administration. **Tingwen Zhou:** Methodology. **Weihua Qiao:** Methodology. **Jiawei Shi:** Project administration, Methodology. **Fei Li:** Resources, Project administration. **Li Xu:** Writing – review & editing, Visualization. **Yuming Huang:** Writing – review & editing, Resources, Conceptualization. **Nianguo Dong:** Writing – review & editing, Resources.

Declaration of competing interest

The authors declare that they have no known competing financial interests or personal relationships that could have appeared to influence the work reported in this paper.

Data availability

I have shared the code for the GEO database used in this study in the Methods section of the manuscript.

Abbreviations

CAVD	calcific aortic valve disease
FOXO1	Forkhead box O1
VICs	valve interstitial cells
HCD	high cholesterol diet
SMURF2	SMAD-specific E3 ubiquitin ligase 2
RUNX2	runt-related transcription factor 2
OM	osteogenic medium
GSEA	gene set enrichment analysis
VSMCs	vascular smooth muscle cells

Appendix A. Supplementary data

Supplementary data to this article can be found online at https://doi.org/10.1016/j.redox.2024.103215.

References

[1] V.T. Nkomo, J.M. Gardin, T.N. Skelton, J.S. Gottdiener, C.G. Scott, M. Enriquez-Sarano, Burden of valvular heart diseases: a population-based study, Lancet 368 (9540) (2006) 1005–1011.
[2] S. Coffey, B. Cox, M.J.A. Williams, The prevalence, incidence, progression, and risks of aortic valve sclerosis, J. Am. Coll. Cardiol. 63 (25) (2014) 2852–2861.
[3] S. Yadgir, C.O. Johnson, V. Aboyans, O.M. Adebayo, R.A. Adedoyin, M. Afarideh, et al., Global, regional, and national burden of calcific aortic valve and degenerative mitral valve diseases, 1990–2017, Circulation 141 (21) (2020) 1670–1680.

[4] Z. Liu, K. Wang, C. Jiang, Y. Chen, F. Liu, M. Xie, et al., Morusin alleviates aortic valve calcification by inhibiting valve interstitial cell senescence through Ccnd1/Trim25/Nrf2 Axis, Adv. Sci (Weinh). (2024) e2307319.
[5] P.R. Goody, M.R. Hosen, D. Christmann, S.T. Niepmann, A. Zietzer, M. Adam, et al., Aortic valve stenosis, Arterioscler. Thromb. Vasc. Biol. 40 (4) (2020) 885–900.
[6] X. Yang, D.A. Fullerton, X. Su, L. Ao, J.C. Cleveland, X. Meng, Pro-osteogenic phenotype of human aortic valve interstitial cells is associated with higher levels of toll-like receptors 2 and 4 and enhanced expression of bone morphogenetic protein 2, J. Am. Coll. Cardiol. 53 (6) (2009) 491–500.
[7] N. Ghosh-Choudhury, S.L. Abboud, R. Nishimura, A. Celeste, L. Mahimainathan, G. G. Choudhury, Requirement of BMP-2-induced phosphatidylinositol 3-kinase and Akt Serine/Threonine Kinase in osteoblast differentiation and Smad-dependent BMP-2 gene transcription, J. Biol. Chem. 277 (36) (2002) 33361–33368.
[8] P. Kaliman, F. Viñals, X. Testar, M. Palacín, A. Zorzano, Phosphatidylinositol 3-Kinase inhibitors block differentiation of skeletal muscle cells, J. Biol. Chem. 271 (32) (1996) 19146–19151.
[9] D. Theofilatos, P. Fotakis, E. Valanti, D. Sanoudou, V. Zannis, D. Kardassis, HDL-apoA-I induces the expression of angiopoietin like 4 (ANGPTL4) in endothelial cells via a PI3K/AKT/FOXO1 signaling pathway, Metabolism 87 (2018) 36–47.
[10] H. Dharaneeswaran, M.R. Abid, L. Yuan, D. Dupuis, D. Beeler, K.C. Spokes, et al., FOXO1-Mediated activation of Akt plays a critical role in vascular homeostasis, Circ. Res. 115 (2) (2014) 238–251.
[11] A. Orea-Soufi, J. Paik, J. Bragança, T.A. Donlon, B.J. Willcox, W. Link, FOXO transcription factors as therapeutic targets in human diseases, Trends Pharmacol. Sci. 43 (12) (2022) 1070–1084.
[12] G. Calissi, E.W.F. Lam, W. Link, Therapeutic strategies targeting FOXO transcription factors, Nat. Rev. Drug Discov. 20 (1) (2021) 21–38.
[13] M.J. Rodriguez-Colman, T.B. Dansen, B.M.T. Burgering, FOXO transcription factors as mediators of stress adaptation, Nat. Rev. Mol. Cell Biol. 25 (1) (2024) 46–64.
[14] H. Zhang, Y. Pan, L. Zheng, C. Choe, B. Lindgren, E.D. Jensen, et al., FOXO1 inhibits Runx2 transcriptional activity and prostate cancer cell migration and invasion, Cancer Res. 71 (9) (2011) 3257–3267.
[15] W.J. Moorhead, C.C. Chu, R.A. Cuevas, J. Callahan, R. Wong, C. Regan, et al., Dysregulation of FOXO1 (forkhead box O1 protein) drives calcification in arterial calcification due to deficiency of CD73 and is present in peripheral artery disease, Arterioscler. Thromb. Vasc. Biol. 40 (7) (2020) 1680–1694.
[16] D. Jian, Y. Wang, L. Jian, H. Tang, L. Rao, K. Chen, et al., METTL14 aggravates endothelial inflammation and atherosclerosis by increasing FOXO1 N6-methyladeosine modifications, Theranostics 10 (20) (2020) 8939–8956.
[17] K. Tsuchiya, M. Westerterp, A.J. Murphy, V. Subramanian, A.W. Ferrante, A. R. Tall, et al., Expanded granulocyte/monocyte compartment in myeloid-specific triple FoxO knockout increases oxidative stress and accelerates atherosclerosis in mice, Circ. Res. 112 (7) (2013) 992–1003.
[18] K. Tsuchiya, J. Tanaka, Y. Shuiqing, C.L. Welch, R.A. DePinho, I. Tabas, et al., FoxOs integrate pleiotropic actions of insulin in vascular endothelium to protect mice from atherosclerosis, Cell Metabol. 15 (3) (2012) 372–381.
[19] Z. Liu, N. Dong, H. Hui, Y. Wang, F. Liu, L. Xu, et al., Endothelial cell-derived tetrahydrobiopterin prevents aortic valve calcification, Eur. Heart J. 43 (17) (2022) 1652–1664.
[20] Y. Wang, D. Han, T. Zhou, C. Chen, H. Cao, J.Z. Zhang, et al., DUSP26 induces aortic valve calcification by antagonizing MDM2-mediated ubiquitination of DPP4 in human valvular interstitial cells, Eur. Heart J. 42 (30) (2021) 2935–2951.
[21] S.H. Lee, N. Kim, M. Kim, S. Woo, I. Han, J. Park, et al., Single-cell transcriptomics reveal cellular diversity of aortic valve and the immunomodulation by PPARγ during hyperlipidemia, Nat. Commun. 13 (1) (2022).
[22] M.J. Rodriguez-Colman, T.B. Dansen, B.M.T. Burgering, FOXO transcription factors as mediators of stress adaptation, Nat. Rev. Mol. Cell Biol. 25 (1) (2024) 46–64.
[23] Y. Huang, C. Jiang, L. Chen, J. Han, M. Liu, T. Zhou, et al., Gli1 promotes the phenotypic transformation of valve interstitial cells through Hedgehog pathway activation exacerbating calcific aortic valve disease, Int. J. Biol. Sci. 19 (7) (2023) 2053–2066.
[24] Y. Huang, X. Zhou, M. Liu, T. Zhou, J. Shi, N. Dong, et al., The natural compound andrographolide inhibits human aortic valve interstitial cell calcification via the NF-kappa B/Akt/ERK pathway, Biomed. Pharmacother. 125 (2020) 109985.
[25] M. Liu, F. Li, Y. Huang, T. Zhou, S. Chen, G. Li, et al., Caffeic acid phenethyl ester ameliorates calcification by inhibiting activation of the AKT/NF-κB/NLRP3 inflammasome pathway in human aortic valve interstitial cells, Front. Pharmacol. 11 (2020).
[26] T. Zhou, Y. Wang, M. Liu, Y. Huang, J. Shi, N. Dong, et al., Curcumin inhibits calcification of human aortic valve interstitial cells by interfering NF-κB, AKT, and ERK pathways, Phytother Res. 34 (8) (2020) 2074–2081.
[27] J. Yu, W. Sun, Z. Wang, X. Liang, F. Hua, K. Li, et al., TRIB3 supports breast cancer stemness by suppressing FOXO1 degradation and enhancing SOX2 transcription, Nat. Commun. 10 (1) (2019).
[28] L. Deng, L. Huang, Y. Sun, J.M. Heath, H. Wu, Y. Chen, Inhibition of FOXO1/3 promotes vascular calcification, Arterioscler. Thromb. Vasc. Biol. 35 (1) (2015) 175–183.
[29] G.M. Novaro, R. Katz, R.J. Aviles, J.S. Gottdiener, M. Cushman, B.M. Psaty, et al., Clinical factors, but not C-reactive protein, predict progression of calcific aortic-valve disease: the cardiovascular Health study, J. Am. Coll. Cardiol. 50 (20) (2007) 1992–1998.
[30] S. Tsimikas, Potential causality and emerging medical therapies for lipoprotein(a) and its associated oxidized phospholipids in calcific aortic valve stenosis, Circ. Res. 124 (3) (2019) 405–415.
[31] K. Xu, S. Xie, Y. Huang, T. Zhou, M. Liu, P. Zhu, et al., Cell-type transcriptome atlas of human aortic valves reveal cell heterogeneity and endothelial to mesenchymal transition involved in calcific aortic valve disease, Arterioscler. Thromb. Vasc. Biol. 40 (12) (2020) 2910–2921.
[32] E. Aikawa, P. Libby, A rock and a hard place: chiseling away at the multiple mechanisms of aortic stenosis, Circulation 135 (20) (2017) 1951–1955.
[33] S. Kraler, M.C. Blaser, E. Aikawa, G.G. Camici, T.F. Luscher, Calcific aortic valve disease: from molecular and cellular mechanisms to medical therapy, Eur. Heart J. 43 (7) (2022) 683–697.
[34] X. Yang, X. Qu, X. Meng, M. Li, D. Fan, T. Fan, et al., MiR-490-3p inhibits osteogenic differentiation in thoracic ligamentum flavum cells by targeting FOXO1, Int. J. Biol. Sci. 14 (11) (2018) 1457–1465.
[35] F. Schlotter, A. Halu, S. Goto, M.C. Blaser, S.C. Body, L.H. Lee, et al., Spatiotemporal multi-omics mapping generates a molecular atlas of the aortic valve and reveals networks driving disease, Circulation 138 (4) (2018) 377–393.
[36] T. Nagashima, N. Shigematsu, R. Maruki, Y. Urano, H. Tanaka, A. Shimaya, et al., Discovery of novel forkhead box O1 inhibitors for treating type 2 diabetes: improvement of fasting glycemia in diabeticdb/db mice, Mol. Pharmacol. 78 (5) (2010) 961–970.
[37] R.J. Deshaies, C.A.P. Joazeiro, RING domain E3 ubiquitin ligases, Annu. Rev. Biochem. 78 (1) (2009) 399–434.
[38] J.J. Smit, T.K. Sixma, RBR E3-ligases at work, EMBO Rep. 15 (2) (2014) 142–154.
[39] V. Khedgikar, P. Kushwaha, J. Gautam, A. Verma, B. Changkija, A. Kumar, et al., Withaferin A: a proteasomal inhibitor promotes healing after injury and exerts anabolic effect on osteoporotic bone, Cell Death Dis. 4 (8) (2013) e778-e778.
[40] A. Durand, N. Bonilla, T. Level, Z. Ginestet, A. Lombès, V. Guichard, et al., Type 1 interferons and Foxo1 down-regulation play a key role in age-related T-cell exhaustion in mice, Nat. Commun. 15 (1) (2024).
[41] C. Castaño, M. Mirasierra, M. Vallejo, A. Novials, M. Párrizas, Delivery of muscle-derived exosomal miRNAs induced by HIIT improves insulin sensitivity through down-regulation of hepatic FoxO1 in mice, Proc. Natl. Acad. Sci. USA 117 (48) (2020) 30335–30343.
[42] Y. Song, L. Wu, M. Li, X. Xiong, Z. Fang, J. Zhou, et al., Down-regulation of MicroRNA-592 in obesity contributes to hyperglycemia and insulin resistance, EBioMedicine 42 (2019) 494–503.
[43] L. Hortells, C. Sosa, N. Guillén, S. Lucea, Á. Millán, V. Sorribas, Identifying early pathogenic events during vascular calcification in uremic rats, Kidney Int. 92 (6) (2017) 1384–1394.
[44] C. Ciavarella, E. Gallitto, F. Ricci, M. Buzzi, A. Stella, G. Pasquinelli, The crosstalk between vascular MSCs and inflammatory mediators determines the pro-calcific remodelling of human atherosclerotic aneurysm, Stem Cell Res. Ther. 8 (1) (2017).
[45] P. Petsophonsakul, M. Burgmaier, B. Willems, S. Heeneman, N. Stadler, F. Gremse, et al., Nicotine promotes vascular calcification via intracellular Ca2+-mediated, Nox5-induced oxidative stress, and extracellular vesicle release in vascular smooth muscle cells, Cardiovasc. Res. 118 (9) (2022) 2196–2210.
[46] S. Cheng, B. Ramachandran, A. Behrmann, J. Shao, M. Mead, C. Smith, et al., Vascular smooth muscle LRP6 limits arteriosclerotic calcification in diabetic LDLR−/− mice by restraining noncanonical wnt signals, Circ. Res. 117 (2) (2015) 142–156.
[47] L. Simard, N. Côté, F. Dagenais, P. Mathieu, C. Couture, S. Trahan, et al., Sex-related discordance between aortic valve calcification and hemodynamic severity of aortic stenosis, Circ. Res. 120 (4) (2017) 681–691.
[48] E. Maher, Aortic and mitral valve calcification in patients with end-stage renal disease, Lancet 330 (8564) (1987) 875–877.
[49] E. Aikawa, M. Aikawa, P. Libby, J. Figueiredo, G. Rusanescu, Y. Iwamoto, et al., Arterial and aortic valve calcification abolished by elastolytic cathepsin S deficiency in chronic renal disease, Circulation 119 (13) (2009) 1785–1794.
[50] J.D. Hutcheson, C. Goettsch, Cardiovascular calcification heterogeneity in chronic kidney disease, Circ. Res. 132 (8) (2023) 993–1012.